Letter

Anomalous lattice relaxation dynamics in optimally doped $La_{2-x}Sr_xCuO_4$

A. N. Petsch,[1,2,*] L. Shen,[1,3,*,†] Z. Porter,[1,2] A. Alshemi,[3] A. Stellhorn,[3] A. Israelski,[1,2] C. Peng,[1,2] H. Yavas,[1] V. Thampy,[1] R. J. Arthur,[1] Z. Ren,[4] F. Westermeier,[4] M. Sprung,[4] S. M. Hayden,[5] E. Blackburn,[3,‡] and J. J. Turner[1,2,§]

[1]*SLAC National Accelerator Laboratory, Menlo Park, California 94025, USA*
[2]*Stanford Institute for Materials and Energy Sciences, Stanford University, Stanford, California 94305, USA*
[3]*Division of Synchrotron Radiation Research, Department of Physics, Lund University, SE-22100 Lund, Sweden*
[4]*Deutsches Elektronen-Synchrotron DESY, Notkestraße 85, D-22607 Hamburg, Germany*
[5]*H.H. Wills Physics Laboratory, University of Bristol, Bristol BS8 1TL, United Kingdom*

(Received 16 February 2025; revised 3 August 2025; accepted 21 August 2025; published 18 September 2025)

The atomic lattice plays a critical role in the emergence of high-T_c superconductivity in cuprates. While the dynamics associated with electron-lattice coupling typically unfold on picosecond-to-femtosecond timescales, we present an x-ray photon correlation spectroscopy investigation on an optimally doped La-based cuprate that reveals a strong response of kilosecond-scale lattice relaxation dynamics to the superconducting state. Notably, an anomaly emerges around T_c: upon cooling into the superconducting state, the average atomic relaxation lifetime decreases, i.e., dynamics accelerate. This indicates a significant change in the local disorder-induced strain field dynamics at the superconducting transition, highlighting a remarkable coupling between superconductivity and the lattice on quasistatic timescales.

DOI: 10.1103/9sg4-52qz

All high-T_c cuprate superconductors are inherently disordered due to carrier doping, which inevitably introduces defects into the crystal lattice. Understanding the interplay between the defects and electronic properties in these materials—such as superconductivity, charge-density waves (CDWs), and the pseudogap—is a central issue and has been the subject of extensive study. Notably, both CDWs and the pseudogap are found to be highly sensitive to certain types of defects [1,2], whereas the superconductivity appears, perhaps counterintuitively, to be relatively robust [3], and in some cases even enhanced [4], in the presence of disorder. Despite this, the direct interaction between superconductivity and lattice disorder remains largely underexplored experimentally. From an experimental standpoint, it is still far from clear how superconductivity can persist and even thrive in a disordered lattice.

In addition to static quenched disorder, defects also induce local atomic relaxation, which can be viewed as a form of dynamic disorder that governs the temporal stability of the host lattice where the defects reside [5]. Typically, relaxation dynamics are thermally activated and can be described by the Arrhenius model:

$$\tau = \tau_0 \exp(\Delta E / k_B T), \tag{1}$$

where ΔE is the thermal activation energy associated with defect pinning and disorder, and τ_0 is the intrinsic relaxation time in the absence of thermal activation [6,7]. Notably, a recent study on $YBa_2Cu_3O_{6+y}$ (YBCO) revealed that Eq. (1) is plainly insufficient to accurately describe the atomic relaxation dynamics inside the superconducting state [8]. This deviation from Arrhenius behavior serves as a '*smoking gun*' for a direct, dynamic coupling between defects and superconductivity—one that potentially sets the upper limit for the temporal coherence of high-T_c superconducting state on quasistatic timescales. This observation raises an important question: Are such anomalous atomic relaxation dynamics ubiquitous across all cuprate superconductors? If so, what are the underlying commonalities and distinctions, particularly in La-based cuprates, where structural degrees of freedom and the associated electronic phenomena are further complicated by multiple types of lattice symmetry-breaking upon cooling [9,10]?

In this Letter, we investigate the atomic lattice relaxation in $La_{2-x}Sr_xCuO_4$ (LSCO). Previous studies have revealed a strong interplay between CDWs and relaxation dynamics in underdoped LSCO [11,12]. To isolate the influence of superconductivity, we focus on optimally doped LSCO ($x = 0.16$, $T_c = 37.6$ K [9]), where CDWs are strongly suppressed [13]. We observe a clear coupling between the onset of superconductivity and the relaxation of the local strain field. Specifically, the mean atomic relaxation lifetime decreases below T_c. These results indicate that the stabilization of the

*These two authors contributed equally to this work.
†Contact author: lingjias@slac.stanford.edu
‡Contact author: elizabeth.blackburn@sljus.lu.se
§Contact author: joshuat@slac.stanford.edu

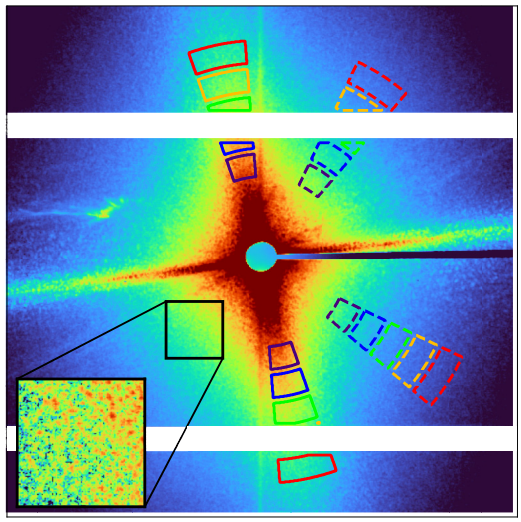

FIG. 1. X-ray diffuse scattering at 27 K. The anisotropic scattering is clearly visible with the major axis canted by about 8 ° from the vertical axis. The sharp, nearly horizontal, feature is a truncation rod [12]. The solid (dashed) boxes show the different ROIs utilized in this work (main text). Horizontal white areas and the round circle in the center mark spaces between detector modules and the beam stop, respectively.

superconducting state is accompanied by enhanced atomic relaxational fluctuations, supporting the notion that anomalous atomic relaxation is a ubiquitous feature in cuprates.

A LSCO ($x = 0.16$) single crystal, which was grown by the optical floating zone technique and cleaved to have the (00L)-plane exposed, was used. Hard x-ray diffraction (HXRD, 8.8 keV) measurements were carried out at the beamline 17-2 at the Stanford Synchrotron Radiation Lightsource (SSRL). Atomic relaxation dynamics were measured by x-ray photon correlation spectroscopy (XPCS)—a method that compares pairs of coherent x-ray diffraction patterns (speckles) resulting from a given structure to probe fluctuations in the time domain [14,15]. These measurements were performed at the coherence applications beamline P10 at the PETRA III facility at the Deutsches Elektronen-Synchrotron DESY, Germany. The x-ray energy was 8.76 keV; the size of the x-ray beam was $2.5 \times 2.5\,\mu m^2$ in full width at half maximum. At each temperature, XPCS time series were performed over a time period of 3600 s with an exposure time of 1 second every 2 seconds. All reflections studied in this work follow the high-temperature tetragonal (HTT) notation (space group $I4/mmm$) [9].

The atomic relaxation in LSCO originates from the local strain field induced by hole doping [16]. At low temperatures, this strain field is governed by a monoclinic distortion [12]. It is associated with the irreducible representations X_1^+ and X_4^+ of the HTT phase, although the precise space group remains undetermined [17]. The existence of monoclinicity in optimally doped LSCO ($x = 0.16$) is confirmed by HXRD (see Supplemental Material [18]).

As in the underdoped compound ($x = 0.12$) [12], the monoclinic distortion leads to a strongly anisotropic diffuse scattering profile near the (0, 0, 4) Bragg reflection. This is shown in the main panel of Fig. 1, where the Bragg peak itself is masked by a beam stop to prevent detector saturation and potential damage. Three distinct features are evident: a broad oval-shaped scattering profile, a sharp streak-like feature, and well-defined speckles visible in the single-shot frame (Fig. 1, inset). The sharp streak is a crystal truncation rod resulting from step formation during the cleaving process and has been reported previously [12]; the related diffuse scattering region has been excluded from the analysis below. In contrast, the broad, oval-shaped scattering is an intrinsic feature that only develops in the monoclinic phase. It has also been observed in underdoped LSCO ($x = 0.12$), where it has been attributed to Huang scattering [12].

Atomic relaxation dynamics can be probed by analyzing speckle decorrelation in the diffuse scattering region. To this end, regions of interest (ROIs) at various radii (q) from the central Bragg reflection are selected, both within the intense scattering regime along the principal anisotropy axis and in regions far away from it. These ROIs are outlined by solid and dashed lines in Fig. 1 and are used consistently across all temperatures. Selecting ROIs at angles farther from the major axis is limited by the presence of unwanted scattering artifacts, such as truncation rods or irregular features. These artifacts only appear at certain temperatures, likely due to slight shifts in the beam position on the sample surface caused by thermal expansion.

For each pair of ROIs, which are defined by their radial positions q and azimuthal angles relative to the anisotropy axis, the intensity-intensity autocorrelation function $g^{(2)}(\mathbf{Q}, \Delta t)$ is computed using the two-time correlation matrix method described in Ref. [12], where $\Delta t = t_2 - t_1$ is the time delay between two measured scattering patterns. This function captures the correlation between speckle intensities I recorded at two different times t_1 and t_2 via coherent x-ray scattering, thereby reflecting the underlying atomic relaxation dynamics. The uncertainty in $g^{(2)}(\mathbf{Q}, \Delta t)$ is estimated as the standard deviation of all matrix elements $g^{(2)}(\mathbf{Q}, t_1, t_2)$ that satisfy $t_2 - t_1 = \Delta t$. Example $g^{(2)}$ curves (squares) for one value of q and four representative temperatures are shown in Fig. 2, with additional datasets provided in the Supplemental Material [18].

The $g^{(2)}$ functions can be expressed in terms of the contrast $\beta(\mathbf{Q})$ and the normalized intermediate scattering function $F(\mathbf{Q}, \Delta t)$ via the Siegert relation: $g^{(2)}(\mathbf{Q}, \Delta t) \approx 1 + \beta(\mathbf{Q})|F(\mathbf{Q}, \Delta t)|^2$. Here, $\beta(\mathbf{Q}) \leqslant 1$ is a parameter that depends on both the instrument and sample, while $F(\mathbf{Q}, \Delta t)$ is purely sample dependent. A visual inspection of the data reveals that at temperatures well below $T_c \approx 38$ K, the dynamics are significantly faster than those at higher temperatures. The slowest relaxation is observed near T_c, suggesting the breakdown of thermally activated relaxation process [Eq. (1)] at the onset of superconductivity.

In order to quantify the relaxation dynamics, the $|F(\mathbf{Q}, \Delta t)|^2$ data are fitted to the Kohlrausch–Williams–Watts (KWW) decay model [12]. In our final analysis, a single KWW channel can reproduce most of the experimental data. In combination with the aforementioned Siegert relation, $g^{(2)}$ can be written as $g^{(2)} \approx c + \beta \exp[-2(\Delta t/\tau)^\gamma]$, where τ is the decay time and γ is the decay exponent. The constant term c is used to account for small deviations from $c = g^{(2)}(\Delta t \to \infty) = 1$, which can arise from instrumental issues, higher-order contributions, or additional decay(s) [19]. We show the respective fits (solid lines) for the exemplary $g^{(2)}$ values in

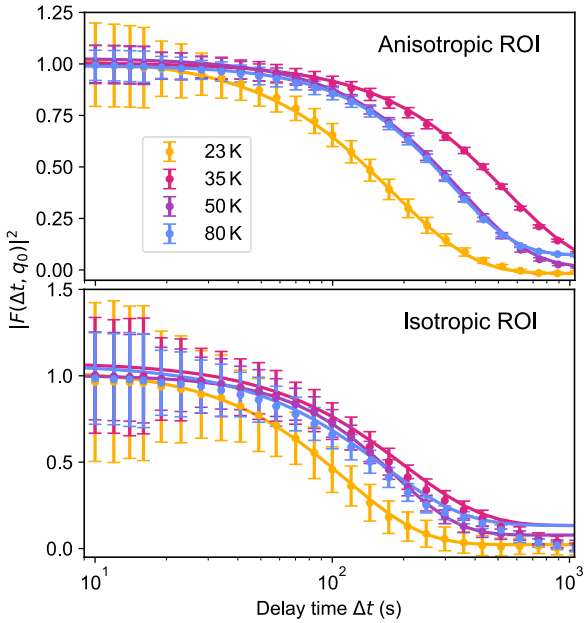

FIG. 2. $|F(\Delta t, q_0 = 3.5 \times 10^{-2}\,\text{Å}^{-1})|^2$ at four relevant temperatures (23 K $< T_c$, 35 K close to T_c, and 50 K and 80 K $> T_c$) with logarithmic binning of time delay steps (for visibility purposes only); Solid lines show the fits to the Siegert relation for $g^{(2)}$; The longest relaxation times arise close to T_c (35 K) while above and below that fastest relaxation times are observed with the fastest at lowest T.

Fig. 2, which provide good descriptions at most temperatures and only show small deviations at long time delays for the isotropic ROI. At all temperatures analyzed, we obtain a compressed decay with an exponent of $\gamma \approx 1.2 \sim 1.6$ (see Supplemental Material [18]). This compressed KWW decay ($\gamma > 1$), which has also been observed in underdoped LSCO [12] and YBCO [8], is typically associated with collective fluctuations in jammed systems [20–22].

Figure 3 presents the main results. Across all q values, the lifetime τ gradually increases as the temperature approaches T_c from above [Fig. 3(a)], consistent with the Arrhenius model described in Eq. (1). A fit to the temperature dependence of τ above T_c yields a weighted average for the local activation energy barrier of $\Delta E \approx 4$ meV (see Supplemental Material [18]). Strikingly, τ reaches a maximum at T_c and then decreases monotonically upon further cooling. This behavior marks a clear departure from the expectations of thermally activated atomic relaxation, suggesting a fundamental change in the underlying dynamics induced by superconductivity.

Moreover, τ exhibits an approximate q^{-1} scaling at all temperatures [Fig. 3(b)], indicating that the relaxation time is inversely proportional to the momentum transfer: $\tau(T, q) \approx A(T) \times q^{-1}$. Such behavior is characteristic of hyperdiffusive dynamics [23,24] or ballistic motion [25]. Accordingly, the proportionality constant $A(T)$ can be interpreted as the inverse of a characteristic velocity of motion, with a unit of seconds per angstrom. This parameter is plotted as a function of temperature in Fig. 3(c) and its inverse, so in units of velocity, is depicted and further discussed in the Supplemental Material [18]. As expected from the $\tau \propto q^{-1}$ scaling, $A(T)$ mirrors the temperature dependence of τ, displaying a pronounced anomaly near T_c. This reinforces the central observation of this work: that the atomic relaxation dynamics in optimally doped LSCO ($x = 0.16$)—as captured by anisotropic diffuse scattering speckles (Fig. 1) [12]—become anomalous upon entering the superconducting state (Fig. 3), while still retaining characteristics of ballistic or hyperdiffusive motion. In the following, we discuss the broader implications of these findings.

We begin with the signature anisotropic Huang scattering, which is the dominant contributor to the observed speckle intensity (Fig. 1). In general, Huang scattering arises from local strain field induced by disorder, such as defects or dislocation loops. In underdoped LSCO ($x = 0.12$), it appears concurrently with the emergence of monoclinic lattice distortions [12,17]. Given that similar monoclinic distortions are observed in the present study, we propose an analogous mechanism for optimally doped LSCO ($x = 0.16$). These

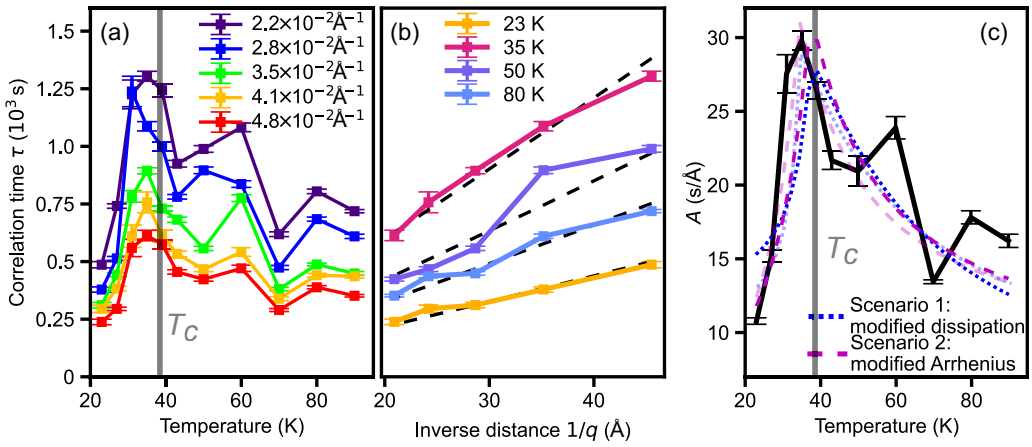

FIG. 3. KWW decay lifetime τ. (a) τ as a function of T at five different q values, showing a maximum near T_c (gray line). (b) τ as a function of q^{-1} with fits to $\tau = A(T)/q$ (black dashed lines, see Supplemental Material [18] for details). (c) $A(T)$ vs temperature, showing a peak near T_c and a sharp decrease on further cooling. The blue dotted line is a fit to Eq. (3) and the violet dashed line to Eq. (4) with $T_c = 37.6$ K and the faint lines are fits of the same functions with $T_c = 34.6$ K (main text).

distortions occur even as the bulk-averaged crystal structure remains largely described by the low-temperature orthorhombic (LTO) phase, indicating that the monoclinic features are subtle. Nonetheless, they produce a substantial amount of Huang scattering, which persists down to the lowest measured temperature (23 K). This persistence suggests that the monoclinic distortions form preferably around defects, defining their structural symmetry, and may themselves constitute a type of disorder relative to the average lattice. The speckle pattern in the diffuse scattering thus provides a direct probe of the local atomic environment around disorder, which is well known for influencing the electronic properties in cuprates [1–4].

At all temperatures studied, the intermediate scattering function is best described by a compressed KWW decay, $\gamma \approx 1.5$, and the relaxation lifetime τ exhibits a q^{-1} scaling. This combination is often associated with internal stress relaxation or shear-relaxation processes in materials with high particle densities [15,20,26–28]. Our sample falls into this category, as local strain fields in LSCO are expected to be percolative at $x = 0.16$, due to the high dopant concentration [16]. In such scenarios, the dynamics observed by XPCS are not diffusive, but rather indicative of ballistic-like motion or avalanche-type transformations in the order parameter. These include processes such as multiatomic displacements, relaxation of internal stress fields [15,20,26,28–31], or step-wise domain wall creep [31,32]. One archetypal mechanism is the so-called slip avalanche, in which atoms collectively overcome a multisided local threshold, releasing stress that is then redistributed through the lattice. Similarly, domain wall creep or domain growth proceeds via thermally activated jumps between local pinning barriers. This is an inherent stepwise process governed by the presence of defects and heterogeneity in the local environment. Crucially, such pinning effects, if coupled to the electronic degrees of freedom, can also influence charge transport, as seen in $La_{1.48}Nd_{0.4}Sr_{0.12}CuO_4$ [11]. This further supports the notion that the atomic relaxation dynamics observed here are intimately linked to the electronic properties of the cuprates [8,12].

We therefore conclude that the probed atomic fluctuations arise from the relaxation of local strain fields in the presence of defects, and they reflect the dynamics of the local lattice environment on quasistatic timescales. In the normal state where the crystal structure is monoclinic, the observed temperature dependence should stem from two processes: (1) thermal fluctuations governed by the Arrhenius model [Eq. (1)], where ΔE represents a local pinning threshold [6,7], and (2) the formation and stabilization of CDWs [12]. Notably, in optimally doped LSCO ($x = 0.16$), the CDW contribution to atomic relaxation is significantly weaker than that in underdoped LSCO ($x = 0.12$) [12], likely due to the much shorter coherence length of the CDW state [13]. As a result, CDW domains never grow large enough to meaningfully influence the relaxation dynamics. Consequently, the temperature dependence in the normal state is well described by the Arrhenius model alone, with the key feature that $A\,(T)$ increases as temperature decreases [Fig. 3(c)].

Below T_c, however, the measured dynamics deviate significantly from the Arrhenius description, representing the most striking observation of this study. Phenomenologically, the observed decrease in τ or $A\,(T)$ [Figs. 3(a) and 3(c)] indicates a temporal destabilization of local strain fields. We propose that this anomaly arises from a coupling between the superconducting and lattice order parameters, ψ_{SC} and ψ_{L}. Such coupling could modify either the intrinsic relaxation time τ_0 (Scenario 1) or the activation energy threshold ΔE (Scenario 2) of the Arrhenius model [Eq. (1)]. As demonstrated in Ref. [8], where a similar drop in $\tau\,(T)$ is seen well below T_c in YBCO, Scenario 1 can be modeled using a Ginzburg-Landau (GL) free energy functional that includes a coupling term of strength W between ψ_{SC} and ψ_{L}:

$$F = \sum_{i=\{\mathrm{L,SC}\}} \left(\alpha_i|\psi_i|^2 + \beta_i|\psi_i|^4\right) + W|\psi_{\mathrm{L}}|^2|\psi_{\mathrm{SC}}|^2, \quad (2)$$

where the expansion is up to the quartic order, with $\alpha_{\mathrm{L,SC}}$ and $\beta_{\mathrm{L,SC}}$ as expansion coefficients for their respective order parameters. In this approach, based on the fluctuation-dissipation theorem [33], the renormalized proportionality constant A' can be written as

$$A'(T) = \frac{A_t + A_0 \exp(\Delta E/k_B T)}{1 - \lambda_1 y^2}, \quad (3)$$

where $\lambda_1 = \frac{W|\psi_{\mathrm{SC}}(0)|^2}{-\alpha_{\mathrm{L}}}$ and $y = |\psi_{\mathrm{SC}}(T)|/|\psi_{\mathrm{SC}}(0)|$, A_0 is the high-temperature limit of the Arrhenius term, and A_t is a tunneling term capturing saturation of τ at lowest temperatures. It is temperature-independent for large potential barriers and low temperatures [34] and was found to be significant in YBCO [8] and for antiferromagnetic domain fluctuations in Cr [21].

Scenario 2 involves a modification of the activation energy ΔE in the Arrhenius equation, governed by the differential form $\mathrm{d}\ln(A) = -\Delta E/k_B T^2\,\mathrm{d}T$. We model this as

$$\Delta E(T) = \Delta E_0 \times \max\{1 - \lambda_2 y^2,\ 0\}, \quad (4)$$

where $\lambda_2 = -\frac{W|\psi_{\mathrm{SC}}(0)|^2\alpha_{\mathrm{L}}}{2\beta_{\mathrm{L}}\Delta E_0}$ and ΔE_0 is the activation energy in the normal state. The remaining term in λ_2, $\frac{W|\psi_{\mathrm{SC}}(0)|^2\alpha_{\mathrm{L}}}{2\beta_{\mathrm{L}}}$, approximately represents the energy shift due to coupling ($W \neq 0$) relative to the uncoupled case ($W = 0$). The analytical solution to the differential equation for ΔE is given in the Supplemental Material [18]. This model yields a peak in $A\,(T)$ at T_c and a sharp drop below it for $\lambda_2 > 1$, while recovering standard Arrhenius behavior at $T \geqslant T_c$. Fits for both Scenarios 1 and 2 are shown in Fig. 3(c): solid lines correspond to the nominal $T_c = 37.6\,\mathrm{K}$, and faint lines represent fits using a downshifted effective $T_c = 34.6\,\mathrm{K}$ to match the observed peak in $A(T)$. Both models reproduce the normal-state barrier $\Delta E_0 \approx 4\,\mathrm{meV}$ and display a maximum at or near T_c, followed by a reduction below it.

Scenario 1 captures most of the drop in $A(T)$ below T_c, but tends to flatten at $T \ll T_c$, where $|\psi_{\mathrm{SC}}|$ saturates and the Arrhenius and tunneling terms overwhelm. In contrast, the suppression of ΔE in Scenario 2 fully accounts for the continued decrease in $A\,(T)$ and suggests 'bare' relaxation at low T, such that $A(T \to 0) = A(T \to \infty) = A_0$. This implies that superconductivity may completely overcome defect or domain wall pinning, and leave the intrinsic relaxation process unchanged. While it is plausible that both τ_0 and ΔE are renormalized simultaneously in optimally doped LSCO,

potentially explaining the magnitude and sharpness of the observed change, physics underlying the latter are the dominant factor.

We point out one detail: in our data, the peak in $A(T)$ occurs at about 35 K, slightly below the bulk $T_c = 37.6$ K [9]. We considered whether this could be due to a small temperature offset, e.g., lag in our sample thermometer, but the shift might also hint at a threshold effecta certain minimum superconducting order parameter amplitude is needed to appreciably influence the lattice dynamics. Such a threshold could arise if, for example, the coupling only becomes effective once phase coherence (or a sufficient superfluid density) is established in the sample. This slight discrepancy does not alter our main conclusions, but it is an interesting nuance for future investigation.

Our observation of anomalous slow lattice relaxation in two distinct cuprate families—underdoped YBCO and optimally doped LSCO-indicates that this behavior is a ubiquitous feature of cuprate superconductors driven by a common mechanism. Both systems share a high density of dopant-induced lattice defects that yield jammed, collective strain dynamics, as evidenced by compressed KWW relaxation exponents ($\gamma > 1$). In both materials, the onset of superconductivity leads to a pronounced acceleration of these slow relaxations, manifested as a clear deviation from Arrhenius behavior and a suppression of the characteristic relaxation lifetime τ below T_c. This correlation between superconductivity and defect dynamics unfolds on quasistatic timescales and may be understood theoretically in terms of 'localized holes', which are highly sensitive to the local atomic environment and, crucially, contribute to the superfluid density [35].

The anomalies in atomic relaxation behavior differ in detail: YBCO exhibits a relatively sharp dip in τ at T_c (consistent with a renormalization of the intrinsic relaxation rate [8], Scenario 1), whereas LSCO shows a more gradual yet ultimately larger suppression of τ in the superconducting state (indicative of a reduced activation energy barrier, Scenario 2). These contrasting manifestations likely stem from differences in the lattice structure and disorder landscape of each material rather than fundamentally distinct physics. For example, LSCO hosts local distortions and twinned domains that are known to couple to superconductivity either directly [9] or via intertwined electronic states such as CDWs [12,17]. These features, which are largely absent in the more rigid orthorhombic lattice of YBCO, may allow superconductivity to more effectively 'soften' the lattice, thereby lowering ΔE. In addition, CDWs may contribute to the observed dynamics via their interplay with atomic relaxation [8,12]. A key difference between the two materials is that the CDW order is optimized in underdoped YBCO, whereas it is strongly suppressed in optimally doped LSCO [13]. The absence of a sharp dip in τ at T_c in LSCO ($x = 0.16$) may therefore be attributed to the suppression of CDW correlations. Disentangling these mechanisms will require theoretical developments beyond the mean-field GL framework, such as incorporating spatiotemporal fluctuations or microscopically modeling how superconducting condensation energy interacts with local strain fields.

In conclusion, by probing lattice relaxation dynamics in a La-based high-T_c superconductor with coherent x-rays, we have revealed a pronounced dynamic interplay between superconductivity and the disordered lattice on unprecedented timescales (kiloseconds). These timescales are markedly slower than those typically associated with the coupling between superconductivity and the lattice [36,37]. Our results provide direct evidence that the superconductivity interacts with lattice disorder dynamically. This insight helps to explain how superconductivity can coexist with (and even benefit from) a disordered lattice—by actively modifying the lattice's temporal behavior. More broadly, our study highlights that electronic and lattice degrees of freedom in cuprates are intertwined not just on ultrafast scales, but even on quasistatic timescales. Such coupling may need to be accounted for in any complete theory of high-T_c superconductivity in disordered crystals.

We acknowledge DESY (Hamburg, Germany), a member of the Helmholtz Association HGF, for the provision of experimental facilities. Parts of this research were carried out at PETRA III, beamline P10. Beamtime was allocated for proposal I-20210586. Use of the Stanford Synchrotron Radiation Lightsource, SLAC National Accelerator Laboratory, is supported by the U.S. Department of Energy, Office of Science, Office of Basic Energy Sciences under Contract No. DE-AC02-76SF00515. L.S., A.A., and E.B. acknowledge support from the Swedish Research Council (Vetenskapsrådet) under Projects No. 201804704 and No. 2024-05899. A.S. acknowledges support from Tillväxtverket. Additionally, part of this work is supported by the Linac Coherent Light Source at SLAC National Accelerator Laboratory, funded by the U.S. Department of Energy, Office of Science, Office of Basic Energy Sciences, under Contract No. DE-AC02-76SF00515. C.P. was supported by the Department of Energy, Office of Science, Basic Energy Sciences, Materials Sciences, and Engineering Division. J.J.T. acknowledges support from the U.S. DOE, Office of Science, Basic Energy Sciences through the Early Career Research Program.

Data availability. The data that support the findings of this article are not publicly available. The data are available from the authors upon reasonable request.

[1] G. Campi, A. Bianconi, N. Poccia, G. Bianconi, L. Barba, G. Arrighetti, D. Innocenti, J. Karpinski, N. D. Zhigadlo, S. M. Kazakov, M. Burghammer, M. v. Zimmermann, M. Sprung, and A. Ricci, Inhomogeneity of charge-density-wave order and quenched disorder in a high-T_c superconductor, Nature (London) **525**, 359 (2015).

[2] I. Zeljkovic, Z. Xu, J. Wen, G. Gu, R. S. Markiewicz, and J. E. Hoffman, Imaging the impact of single oxygen atoms

on superconducting $Bi_{2+y}Sr_{2-y}CaCu_2O_{8+x}$, Science **337**, 320 (2012).

[3] A. Garg, M. Randeria, and N. Trivedi, Strong correlations make high-temperature superconductors robust against disorder, Nat. Phys. **4**, 762 (2008).

[4] J. F. Dodaro and S. A. Kivelson, Generalization of Anderson's theorem for disordered superconductors, Phys. Rev. B **98**, 174503 (2018).

[5] J. C. Qiao and J. M. Pelletier, Dynamic mechanical relaxation in bulk metallic glasses: a review, J. Mater. Sci. Technol. **30**, 523 (2014).

[6] G. Grübel, A. Madsen, and A. Robert, X-ray photon correlation spectroscopy (XPCS), in *Soft Matter Characterization* (Springer, Dordrecht, 2008), pp. 953–995

[7] A. Martinelli, J. Baglioni, P. Sun, F. Dallari, E. Pineda, Y. Duan, T. Spitzbart-Silberer, F. Westermeier, M. Sprung, and G. Monaco, A new experimental setup for combined fast differential scanning calorimetry and x-ray photon correlation spectroscopy, J. Synchrotron Radiat. **31**, 557 (2024).

[8] Z. Porter, L. Shen, R. Plumley, N. G. Burdet, A. N. Petsch, J. Wen, N. C. Drucker, C. Peng, X. M. Chen, A. Fluerasu, E. Blackburn, G. Coslovich, D. G. Hawthorn, and J. J. Turner, Understanding the superconductivity and charge density wave interaction through quasi-static lattice fluctuations, Proc. Natl. Acad. Sci. **121**, e2412182121 (2024).

[9] K. Yamada, C. H. Lee, K. Kurahashi, J. Wada, S. Wakimoto, S. Ueki, H. Kimura, Y. Endoh, S. Hosoya, G. Shirane, R. J. Birgeneau, M. Greven, M. A. Kastner, and Y. J. Kim, Doping dependence of the spatially modulated dynamical spin correlations and the superconducting-transition temperature in $La_{2-x}Sr_xCuO_4$, Phys. Rev. B **57**, 6165 (1998).

[10] M. Hücker, M. v. Zimmermann, G. D. Gu, Z. J. Xu, J. S. Wen, G. Xu, H. J. Kang, A. Zheludev, and J. M. Tranquada, Stripe order in superconducting $La_{2-x}Ba_xCuO_4$ ($0.095 \geqslant x \geqslant 0.155$), Phys. Rev. B **83**, 104506 (2011).

[11] P. G. Baity, T. Sasagawa, and D. Popović, Collective dynamics and strong pinning near the onset of charge order in $La_{1.48}Nd_{0.4}Sr_{0.12}CuO_4$, Phys. Rev. Lett. **120**, 156602 (2018).

[12] L. Shen, V. Esposito, N. G. Burdet, M. Zhu, A. N. Petsch, T. P. Croft, S. P. Collins, Z. Ren, F. Westermeier, M. Sprung, S. M. Hayden, J. J. Turner, and E. Blackburn, Interplay between relaxational atomic fluctuations and charge density waves in $La_{2-x}Sr_xCuO_4$, Phys. Rev. B **108**, L201111 (2023).

[13] T. P. Croft, C. Lester, M. S. Senn, A. Bombardi, and S. M. Hayden, Charge density wave fluctuations in $La_{2-x}Sr_xCuO_4$ and their competition with superconductivity, Phys. Rev. B **89**, 224513 (2014).

[14] S. K. Sinha, Z. Jiang, and L. B. Lurio, X-ray photon correlation spectroscopy studies of surfaces and thin films, Adv. Mater. **26**, 7764 (2014).

[15] A. Madsen, R. L. Leheny, H. Guo, M. Sprung, and O. Czakkel, Beyond simple exponential correlation functions and equilibrium dynamics in x-ray photon correlation spectroscopy, New J. Phys. **12**, 055001 (2010).

[16] J. Q. Lin, X. Liu, E. Blackburn, S. Wakimoto, H. Ding, Z. Islam, and S. K. Sinha, Quantitative characterization of the nanoscale local lattice strain induced by Sr dopants in $La_{1.92}Sr_{0.08}CuO_4$, Phys. Rev. Lett. **120**, 197001 (2018).

[17] R. Frison, J. Küspert, Q. Wang, O. Ivashko, M. v. Zimmermann, M. Meven, D. Bucher, J. Larsen, C. Niedermayer, M. Janoschek, T. Kurosawa, N. Momono, M. Oda, N. B. Christensen, and J. Chang, Crystal symmetry of stripe-ordered $La_{1.88}Sr_{0.12}CuO_4$, Phys. Rev. B **105**, 224113 (2022).

[18] See Supplemental Material at http://link.aps.org/supplemental/10.1103/9sg4-52qz for the low-temperature monoclinic transition, additional XPCS data analysis process, and modified Arrhenius model deduction, and which includes Refs. [17,38].

[19] We have also attempted to fit the deviations from unity in c using a second KWW channel with much longer τ, but we cannot unambiguously determine this term in the fitting due to the low contrast, and hence such terms have been avoided utilizing cutoff times and treating c as a free fitting parameter.

[20] L. Cipelletti, L. Ramos, S. Manley, E. Pitard, D. A. Weitz, E. E. Pashkovski, and M. Johansson, Universal non-diffusive slow dynamics in aging soft matter, Faraday Discuss. **123**, 237 (2002).

[21] O. G. Shpyrko, E. D. Isaacs, J. M. Logan, Y. Feng, G. Aeppli, R. Jaramillo, H. C. Kim, T. F. Rosenbaum, P. Zschack, M. Sprung, S. Narayanan, and A. R. Sandy, Direct measurement of antiferromagnetic domain fluctuations, Nature (London) **447**, 68 (2007).

[22] R. Kukreja, N. Hua, J. Ruby, A. Barbour, W. Hu, C. Mazzoli, S. Wilkins, E. E. Fullerton, and O. G. Shpyrko, Orbital domain dynamics in magnetite below the Verwey transition, Phys. Rev. Lett. **121**, 177601 (2018).

[23] J. Duplat, S. Kheifets, T. Li, M. G. Raizen, and E. Villermaux, Superdiffusive trajectories in Brownian motion, Phys. Rev. E **87**, 020105(R) (2013).

[24] E. Wandersman, Y. Chushkin, E. Dubois, V. Dupuis, A. Robert, and R. Perzynski, Field induced anisotropic cooperativity in a magnetic colloidal glass, Soft Matter **11**, 7165 (2015).

[25] H. Conrad, F. Lehmkühler, B. Fischer, F. Westermeier, M. A. Schroer, Y. Chushkin, C. Gutt, M. Sprung, and G. Grübel, Correlated heterogeneous dynamics in glass-forming polymers, Phys. Rev. E **91**, 042309 (2015).

[26] L. Cipelletti and L. Ramos, Slow dynamics in glassy soft matter, J. Phys.: Condens. Matter **17**, R253 (2005).

[27] J.-P. Bouchaud and E. Pitard, Anomalous dynamical light scattering in soft glassy gels, Eur. Phys. J. E **6**, 231 (2001).

[28] B. Chung, S. Ramakrishnan, R. Bandyopadhyay, D. Liang, C. F. Zukoski, J. L. Harden, and R. L. Leheny, Microscopic dynamics of recovery in sheared depletion gels, Phys. Rev. Lett. **96**, 228301 (2006).

[29] K. A. Dahmen, Y. Ben-Zion, and J. T. Uhl, Micromechanical model for deformation in solids with universal predictions for stress-strain curves and slip avalanches, Phys. Rev. Lett. **102**, 175501 (2009).

[30] M. Zaiser, Scale invariance in plastic flow of crystalline solids, Adv. Phys. **55**, 185 (2006).

[31] E. K. H. Salje and K. A. Dahmen, Crackling noise in disordered materials, Annu. Rev. Condens. Matter Phys. **5**, 233 (2014).

[32] S. Gorfman, A. A. Bokov, A. Davtyan, M. Reiser, Y. Xie, Z.-G. Ye, A. V. Zozulya, M. Sprung, U. Pietsch, and C. Gutt, Ferroelectric domain wall dynamics characterized with x-ray photon correlation spectroscopy, Proc. Natl. Acad. Sci. **115**, E6680 (2018).

[33] R. Kubo, The fluctuation-dissipation theorem, Rep. Prog. Phys. **29**, 255 (1966).

[34] E. M. Chudnovsky and J. Tejada, *Macroscopic Quantum Tunneling of the Magnetic Moment* (Cambridge University Press, Cambridge, 1998)

[35] D. Pelc, P. Popčević, M. Požek, M. Greven, and N. Barišić, Unusual behavior of cuprates explained by heterogeneous charge localization, Sci. Adv. **5**, eaau4538 (2019).

[36] M. Frachet, S. Benhabib, I. Vinograd, S.-F. Wu, B. Vignolle, H. Mayaffre, S. Krämer, T. Kurosawa, N. Momono, M. Oda, J. Chang, C. Proust, M.-H. Julien, and D. LeBoeuf, High magnetic field ultrasound study of spin freezing in $La_{1.88}Sr_{0.12}CuO_4$, Phys. Rev. B **103**, 115133 (2021).

[37] W. A. Atkinson, P. J. Hirschfeld, and A. H. MacDonald, Gap inhomogeneities and the density of states in disordered d-wave superconductors, Phys. Rev. Lett. **85**, 3922 (2000).

[38] B. J. Campbell, H. T. Stokes, D. E. Tanner, and D. M. Hatch, ISODISPLACE: a web-based tool for exploring structural distortions, J. Appl. Crystallogr. **39**, 607 (2006).